

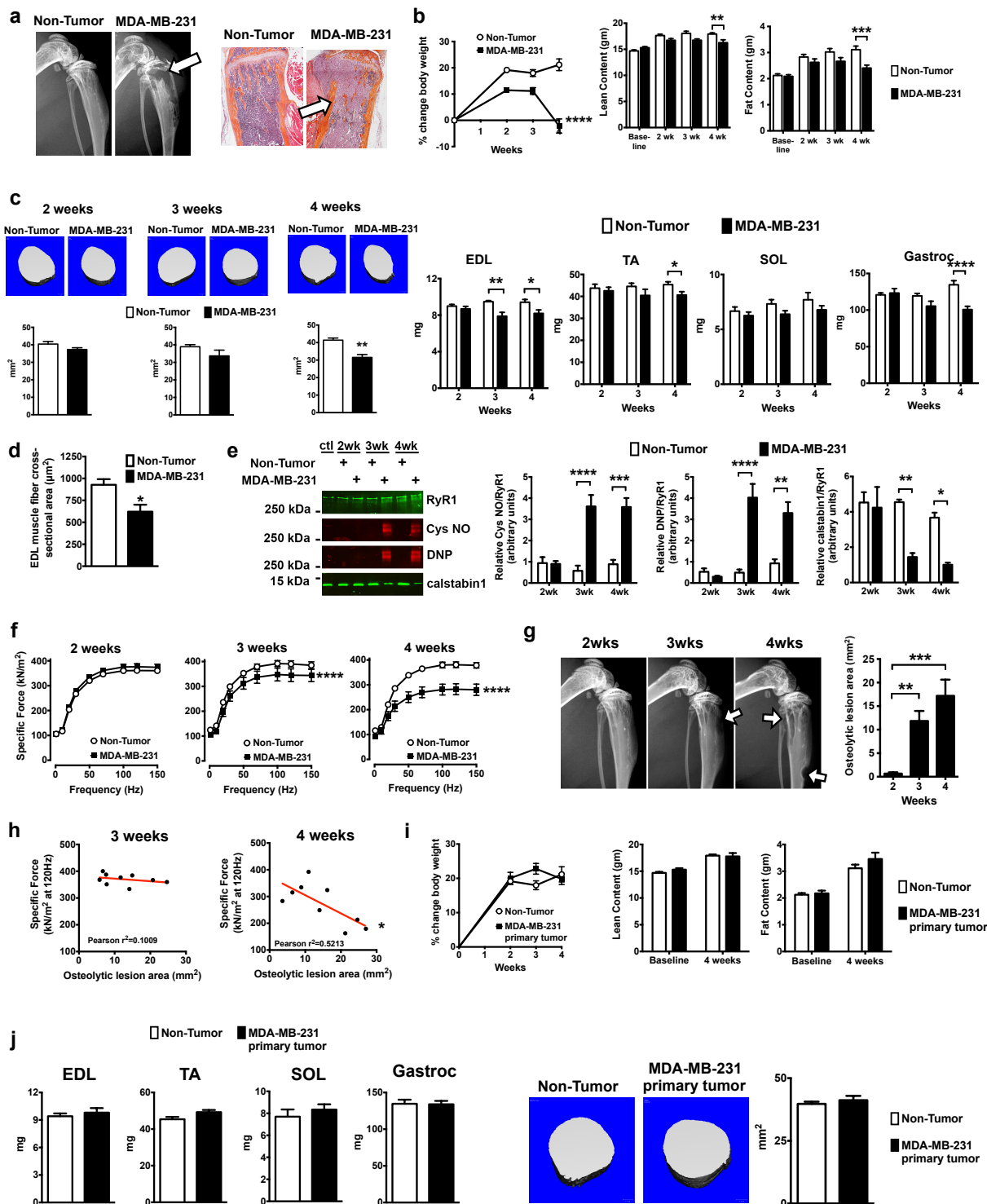
## Supplementary Figures and Tables to

### **Excess TGF- $\beta$ mediates muscle weakness associated with bone metastases in mice**

David L. Waning, Khalid S. Mohammad, Steven Reiken, Wenjun Xie, Daniel C. Andersson, Sutha John, Antonella Chiechi, Laura E. Wright, Alisa Umanskaya, Maria Niewolna, Trupti Trivedi, Sahba Charkhzarrin, Pooja Khatiwada, Anetta Wronska, Ashley Haynes, Maria Serena Benassi, Frank A. Witzmann, Gehua Zhen, Xiao Wang, Xu Cao, G. David Roodman, Andrew R. Marks, Theresa A. Guise

**Supplementary Figures 1-8**

**Supplementary Tables 1-3**



## Supplementary Figure 1

MDA-MB-231 bone metastases but not primary breast cancer lead to progressive weight loss and muscle weakness.

**(a)** left: X-ray analysis revealed large osteolytic lesions (arrows) in mice receiving MDA-MB-231 cells via the intra-cardiac route at 4-weeks post-inoculation. right: MDA-MB-231 tumor cells visible in the bone (arrows) by H&E staining.

**(b)** left: Body weight loss in mice with MDA-MB-231 bone metastases (percent change in total body weight over baseline) ( $n=12$ ). right: Dual energy X-ray absorptiometry (DXA) scan revealed loss of both lean and fat content in mice with bone metastases at 4-weeks post-inoculation ( $n=12$ ).

**(c)** left: Mid-calf cross-sectional area, measured by *in vivo* microCT imaging, was lower in mice with bone metastases at 4-weeks post-inoculation ( $n=5$ ). right: Lower weight of individual muscles dissected from the lower hindlimb ( $n=10$ ) of mice with MDA-MB-231 bone metastases; extensor digitorum longus (EDL), tibialis anterior (TA), soleus (SOL), gastrocnemius (Gastroc) compared to non-tumor control mice.

**(d)** EDL muscle fiber diameter was lower in mice with bone metastases ( $n=200$  fibers from  $n=5$  histological sections) compared to non-tumor control mice.

**(e)** RyR1 was oxidized (DNP) and nitrosylated (CysNO) and RyR1-calstabin1 co-immunoprecipitation from EDL muscle was lower at 3- and 4-weeks post-inoculation ( $n=3$ ) compared to non-tumor control mice.

**(f)** Lower *ex vivo* specific force of the EDL muscle at 3- and 4-weeks post-inoculation ( $n=9$ ) compared to non-tumor control mice.

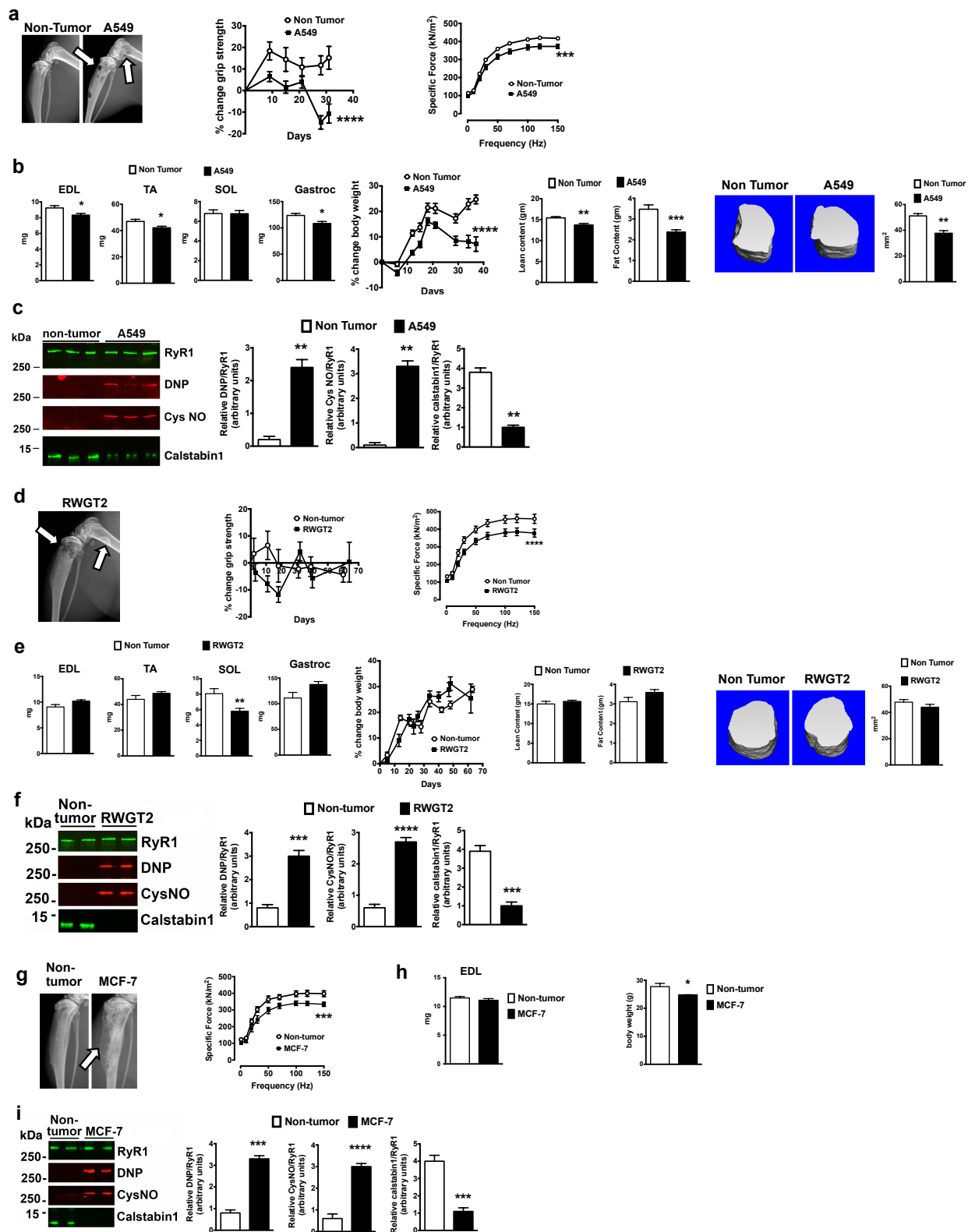
**(g)** Osteolytic lesions and quantitation of lesion area measured by X-ray imaging of all 4 limbs of mice with breast cancer bone metastases at 2, 3 and 4-weeks post-inoculation ( $n=8$ ).

**(h)** Bone destruction correlated to muscle weakness in mice with bone metastases (relationship between specific force (120Hz) and lesion area measured by X-ray imaging) at 4-weeks post-inoculation ( $n=8$ ).

**(i)** left: Mice with MDA-MB-231 primary tumors in the mammary fat pad (without bone metastases) did not have reduced body weight over baseline compared to non-tumor bearing mice ( $n=12$ ). right: Mice with primary tumor did not have altered body composition (DXA scan to measure both lean and fat content in mice) ( $n=9$ ) compared to non-tumor control mice.

**(j)** left: Mice with primary tumor did not have altered individual muscles dissected from the lower hindlimb ( $n=8$ ). right: Mid-calf cross-sectional area was measured by *in vivo* microCT imaging and showed no difference in mice with MDA-MB-231 primary tumors ( $n=10$ ) compared to non-tumor control mice.

Data are mean  $\pm$  s.e.m., **(b,f,i)** Two-way ANOVA; **(b,c,e,g,i)** One-way ANOVA with multiple comparisons; **(c,d,j,j)** t-test; **(h)** Pearson's correlation. \* $P<0.05$ , \*\* $P<0.01$ , \*\*\* $P<0.001$ , \*\*\*\* $P<0.0001$ .



## Supplementary Figure 2

Bone metastases models with osteolytic or mixed osteolytic/osteoblastic bone lesions are associated with muscle weakness.

**(a)** left: A549 bone metastases are osteolytic. middle: *In vivo* forelimb grip strength. right: *Ex vivo* specific force of the EDL muscle are lower in mice with A549 lung cancer bone metastases at 6-weeks post-inoculation ( $n=10$ ) compared to non-tumor control mice.

**(b)** left: Weight of individual muscles dissected from the lower hindlimb at 6-weeks post-inoculation ( $n=10$ ) was lower for EDL, TA and Gastroc muscles compared to non-tumor control mice. middle left: Mice with bone metastases lose weight compared to non-tumor mice ( $n=10$ ). middle right: DXA scan revealed loss of both lean and fat content ( $n=10$ ) compared to non-tumor control mice. right: Mid-calf cross-sectional area, measured by *in vivo* microCT imaging, was lower in mice with bone metastases ( $n=4$ ) compared to non-tumor control mice.

**(c)** RyR1 was oxidized (DNP) and nitrosylated (CysNO) and calstabin1 binding to RyR1 was lower by co-immunoprecipitation from skeletal muscle in mice with A549 bone metastases (EDL;  $n=3$ ) compared to non-tumor control mice.

**(d)** left: RWGT2 bone metastases are osteoblastic/osteolytic. middle: RWGT2 lung cancer bone metastases did not alter forelimb grip strength. right: RWGT2 lung cancer bone metastases lower *ex vivo* EDL specific force ( $n=10$ ) compared to non-tumor control mice.

**(e)** left: Mice with RWGT2 bone metastases did not have altered individual muscle weight (with the exception of soleus) compared to non-tumor control mice. middle left: Body weight (percent change over baseline) in mice with RWGT2 bone metastases compared to non-tumor control mice. middle right: Body composition in mice with RWGT2 bone metastases compared to non-tumor control mice. right: Mid-calf cross-sectional area ( $n=10$ ) in mice with RWGT2 bone metastases compared to non-tumor control mice.

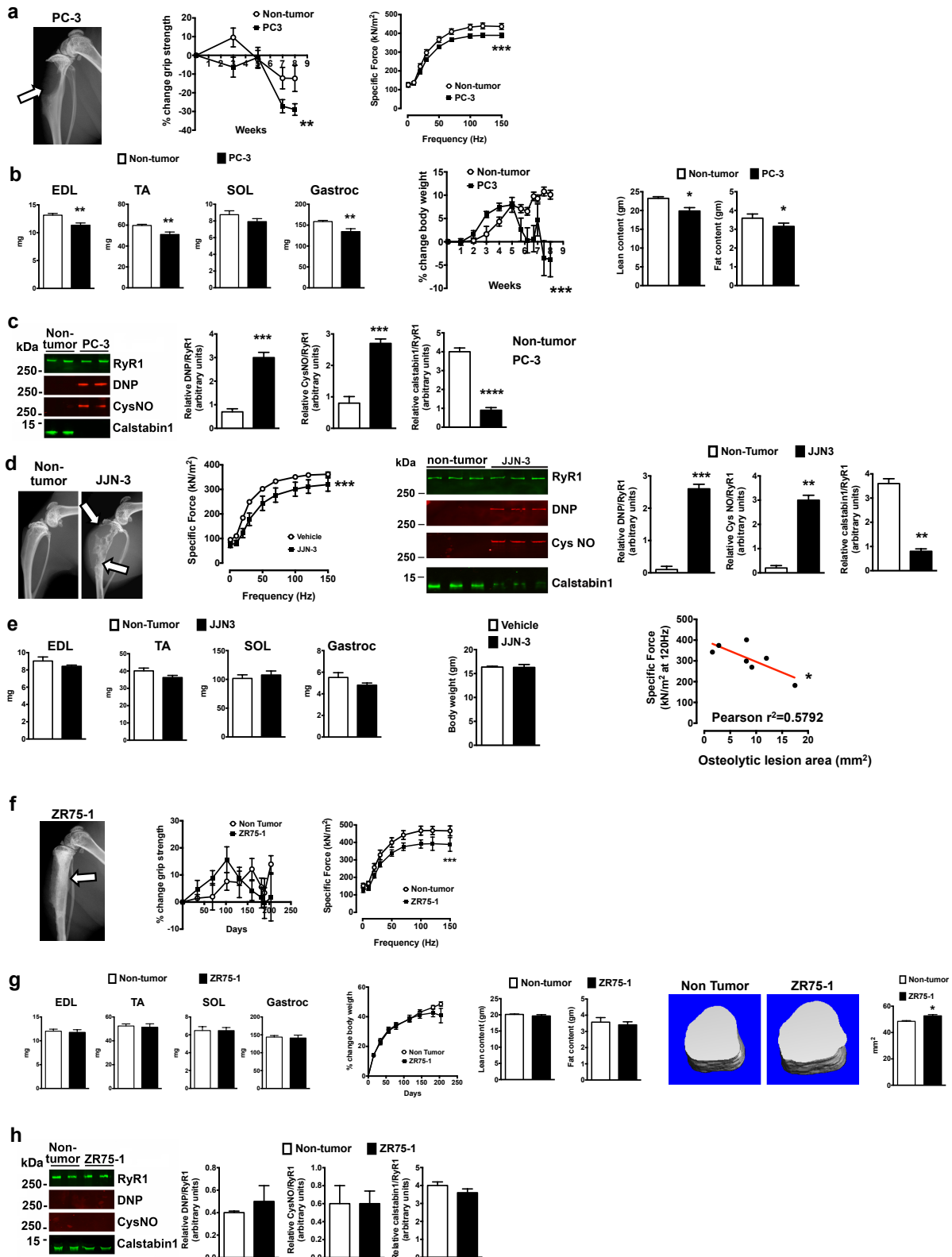
**(f)** RyR1 from muscle of mice with RWGT2 bone metastases was oxidized and nitrosylated and depleted of calstabin1 compared to non-tumor controls ( $n=10$ ).

**(g)** left: MCF-7 breast cancer in bone is osteoblastic/osteolytic. right: Mice with MCF-7 breast cancer in bone caused lower EDL *ex vivo* specific force ( $n=10$ ) compared to non-tumor control mice.

**(h)** EDL muscle weight was not lower in mice with MCF-7 cancer in bone compared to non-tumor control mice. right: Mice with MCF-7 cancer in bone caused lost weight compared to non-tumor control animals.

**(i)** RyR1 was oxidized and nitrosylated and calstabin1 binding was lower in mice with MCF-7 cancer in bone ( $n=4$ ) compared to non-tumor control mice.

Data are mean  $\pm$  s.e.m., **(a,d,e,g)** Two-way ANOVA with Bonferroni multiple comparisons; **(b,c,e,f,h,i)** t-test. \* $P<0.05$ , \*\* $P<0.01$ , \*\*\* $P<0.001$ , \*\*\*\* $P<0.0001$ .



### Supplementary Figure 3

Prostate cancer bone metastases and multiple myeloma cause bone destruction and muscle weakness.

**(a)** left: PC-3 prostate cancer bone metastases are osteolytic. middle: Reduced forelimb grip strength ( $n=8$ ) in mice with PC-3 bone metastases compared to non-tumor control mice. right: *Ex vivo* EDL specific force ( $n=8$ ) in mice with PC-3 bone metastases compared to non-tumor control mice.

**(b)** Mice with PC-3 bone metastases had left: lower individual muscle weight ( $n=8$ ), middle: reduced body weight (percent change over baseline) ( $n=8$ ), right: reduced lean and fat content ( $n=8$ ) compared to non-tumor control mice.

**(c)** RyR1 from skeletal muscle of mice with PC-3 bone metastases was oxidized and nitrosylated and had lower calstabin1 binding to the RyR1 complex compared to non-tumor controls ( $n=4$ ).

**(d)** left: Radiographs showing bone destruction in mice with JJN-3 tumors. middle: *Ex vivo* specific force of the contralateral extensor digitorum longus (EDL) muscle was lower in mice bearing JJN-3 tumor ( $n=6$ ) compared to non-tumor control mice. right: RyR1 was oxidized (DNP) and nitrosylated (CysNO) and calstabin1 binding to RyR1 was lower by co-immunoprecipitation from EDL skeletal muscle ( $n=3$ ) compared to non-tumor control mice.

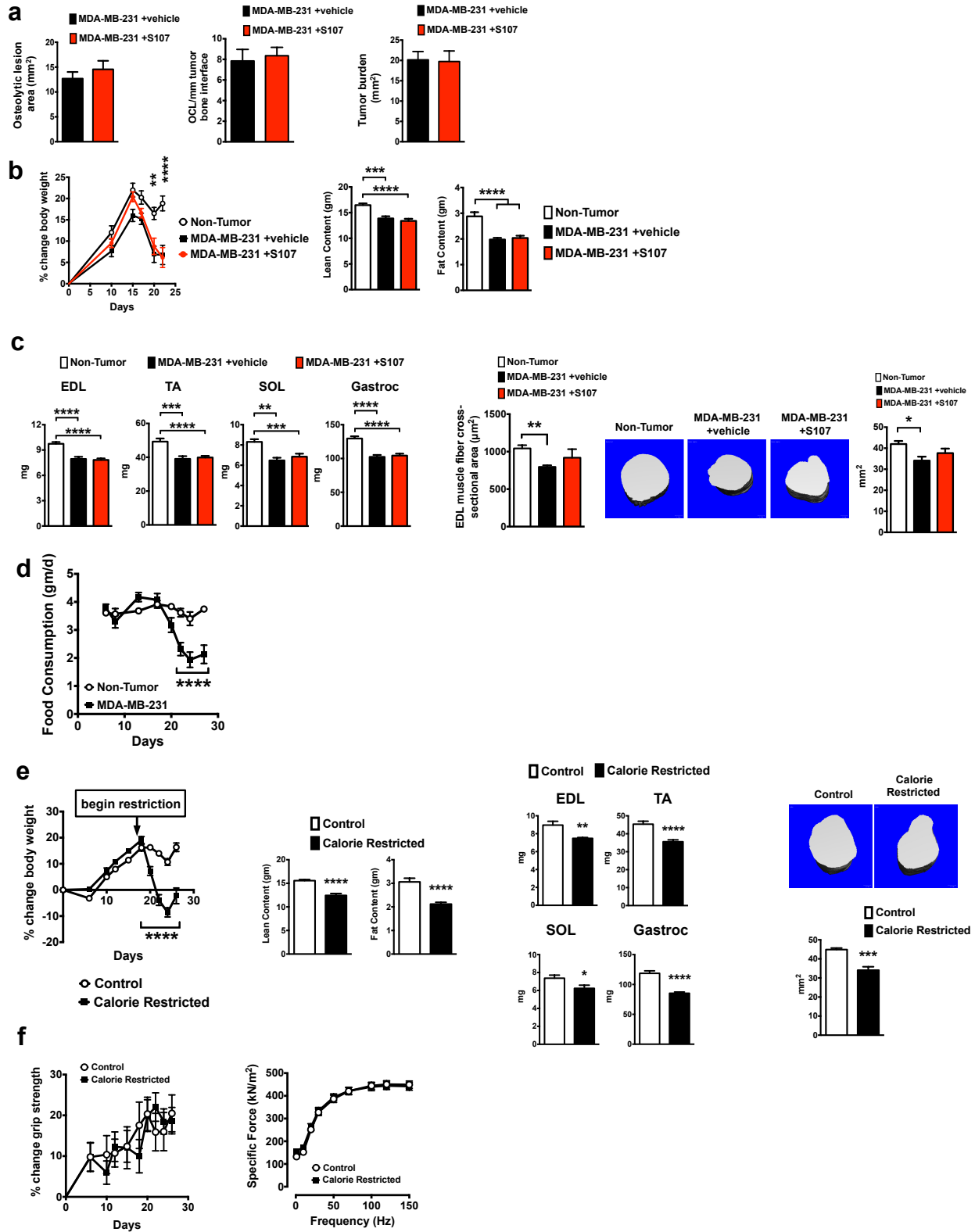
**(e)** left: Weight of individual muscles dissected from the lower hindlimb at 6-weeks post-inoculation ( $n=6$ ) were not changed in mice with JJN-3 cells compared to non-tumor control mice. middle: JJN-3 tumors were not associated with body weight loss (6-weeks post-inoculation) ( $n=6$ ) compared to non-tumor control mice. right: Relationship between specific force (120Hz) and lesion area (measured in all limbs) by X-ray imaging ( $n=7$ ).

**(f)** left: ZR75-1 breast cancer bone metastases are osteoblastic. middle: Mice with ZR75-1 breast cancer bone metastases did not have reduced forelimb grip strength ( $n=10$ ) compared to non-tumor control mice. right: Mice with ZR75-1 breast cancer bone metastases have lower *ex vivo* EDL specific force compared to non-tumor animals ( $n=10$ ).

**(g)** left: Mice with ZR75-1 bone metastases had similar muscle weight ( $n=10$ ) compared to non-tumor control mice. middle left: Body weight ( $n=10$ ), and (middle right); body composition ( $n=10$ ) compared to non-tumor controls. right: Mice with ZR75-1 bone metastases did have increased mid-calf cross-sectional area compared to non-tumor controls ( $n=4$ ).

**(h)** Mice with ZR75-1 bone metastases had lower *ex vivo* EDL specific force but RyR1 was not oxidized or nitrosylated and calstabin1 binding was intact ( $n=10$ ) compared to non-tumor control mice.

Data are mean  $\pm$  s.e.m. **(a,b,d,f,g)** Two-way ANOVA; **(b,c,d,e,g,h)** t-test; **(e)** Pearson's correlation. \* $P<0.05$ , \*\* $P<0.01$ , \*\*\* $P<0.001$ , \*\*\*\* $P<0.0001$ .



## Supplementary Figure 4

Rycal S107 does not affect body weight or tumor burden and muscle weakness is not due to loss of body weight due to food consumption.

**(a)** left: Osteolytic lesion area (assessed by radiographs) in mice with breast cancer bone metastases treated either with vehicle or S107 were similar ( $n=19$ ). middle: Number of osteoclasts (OCL) per mm at the tumor-bone interface (measured by histomorphometry) ( $n=15$ ) in mice treated either with vehicle or S107. right: Tumor burden in mice with breast cancer bone metastases was similar in mice treated with S107 compared with vehicle ( $n=10$ ).

**(b)** left: Percent change in body weight ( $n=10$ ) was reduced in mice with breast cancer bone metastases compared to non-tumor control mice, and was not changed by treatment with either S107 or vehicle. right: DXA scan revealed loss of both lean and fat content in mice with bone metastases and this change is not affected by treatment ( $n=10$ ).

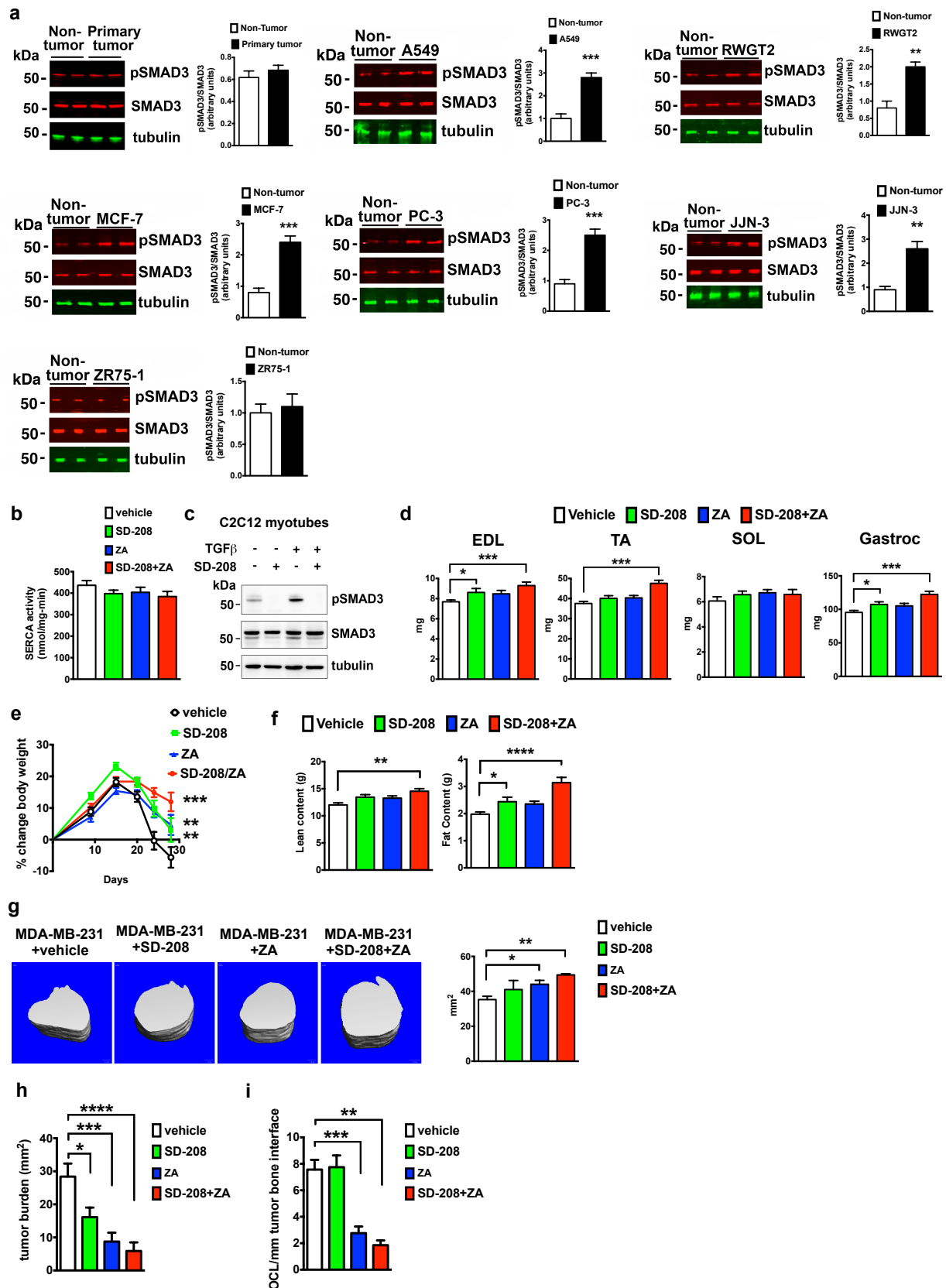
**(c)** left: Weight of individual muscles dissected from the lower hindlimb ( $n=10$ ) was lower in mice with breast cancer bone metastases compared to non-tumor controls and was not affected by treatment. middle: EDL muscle fiber cross-sectional area ( $n=200$  fibers from  $n=3$  histological sections) was lower in mice with breast cancer bone metastases compared to non-tumor controls and was not affected by treatment.. right: Mid-calf cross-sectional area (measured by *in vivo* microCT imaging ( $n=5$ )) was lower in vehicle treated mice with bone metastases compared to non-tumor control mice, but not in mice treated with S107.

**(d)** Mice with breast cancer and bone metastases had reduced food consumption (by up to 40%) in the last week before death. To determine whether muscle weakness in mice with bone metastases was due to reduced food consumption, we restricted food available to normal healthy mice by 30-40% for one week. Despite a significant decrease in body weight due to a loss of both muscle and fat mass, mice subjected to this caloric restriction showed no decrease in forelimb grip strength, and no lowering in EDL muscle specific force compared to pair-fed mice. Mice with bone metastases exhibit reduced food consumption during approximately the last week of life ( $n=8$  cages).

**(e)** left: 30-40% caloric restriction of healthy 8-week-old female nude mice (age matched to last week of bone metastatic models) leads to loss of body weight (calorie restriction initiated at day 18) ( $n=10$ ) compared to pair-fed mice. middle left: Lean and fat content of mice after 1 week of calorie restriction measured by DXA scan ( $n=10$ ) compared to pair-fed mice. middle right: Weight of individual muscles dissected from the lower hindlimb after 1 week of calorie restriction ( $n=10$ ) compared to pair-fed mice. right: *In vivo* mid-calf cross-sectional area of mice after 1 week of calorie restriction ( $n=5$ ) was lower compared to pair-fed mice.

**(f)** left: Forelimb grip strength was not affected by calorie restriction ( $n=10$ ) compared to pair-fed mice. right: *Ex vivo* muscle contractility of the extensor digitorum longus (EDL) muscle was not affected by calorie restriction ( $n=10$ ) compared to pair-fed mice.

Data are mean  $\pm$  s.e.m., **(a,c,e)** t-test; **(b,d,e,f)** Two-way ANOVA; **(b,c)** One-way ANOVA with multiple comparisons. \* $P<0.05$ , \*\* $P<0.01$ , \*\*\* $P<0.001$ , \*\*\*\* $P<0.0001$ .



## Supplementary Figure 5

SMAD3 phosphorylation is higher in mice with osteolytic or mixed osteolytic/osteoblastic bone metastases and muscle weakness; blocking TGF $\beta$ -RI kinase activity (SD-208) or inhibiting bone resorption (ZA) prevented weight loss and lowered tumor burden in muscle from mice with bone metastases.

(a) top row: SMAD3 phosphorylation relative to total SMAD3 was not changed in muscle samples from mice with MDA-MB-231 primary tumors (without bone metastases) compared to non-tumor control mice. SMAD3 phosphorylation was increased in mice with A549 osteolytic lung cancer bone metastases compared to non-tumor control mice, and RWGT2 mixed osteolytic/osteoblastic lung cancer bone metastases ( $n=4$  each) compared to non-tumor control mice. middle row: SMAD3 phosphorylation was increased in MCF-7 mixed osteolytic/osteoblastic breast cancer bone metastases compared to non-tumor control mice, PC-3 osteolytic prostate cancer bone metastases compared to non-tumor control mice, and JJN-3 osteolytic multiple myeloma compared to non-tumor control mice ( $n=4$  each). bottom row: In contrast, SMAD3 phosphorylation relative to total SMAD3 expression in mice with ZR75-1 breast cancer bone metastases was not changed compared to non-tumor control mice.

(b) SERCA activity of mice treated with SD-208, ZA or SD-208+ZA ( $n=4$ ) was not changed compared to vehicle treated mice.

(c) SMAD3 phosphorylation is higher in C2C12 cells treated with TGF $\beta$  and this is blocked by incubation of cells with SD-208.

(d) Muscle weight loss of individual muscles dissected from the lower hindlimb is prevented in mice treated with SD-208, ZA or SD-208+ZA compared to vehicle treated mice ( $n=13$ ).

(e) SD-208, ZA and SD-208+ZA reduce loss of body weight (percent change in body weight over baseline) compared to vehicle treated mice ( $n=15$ ).

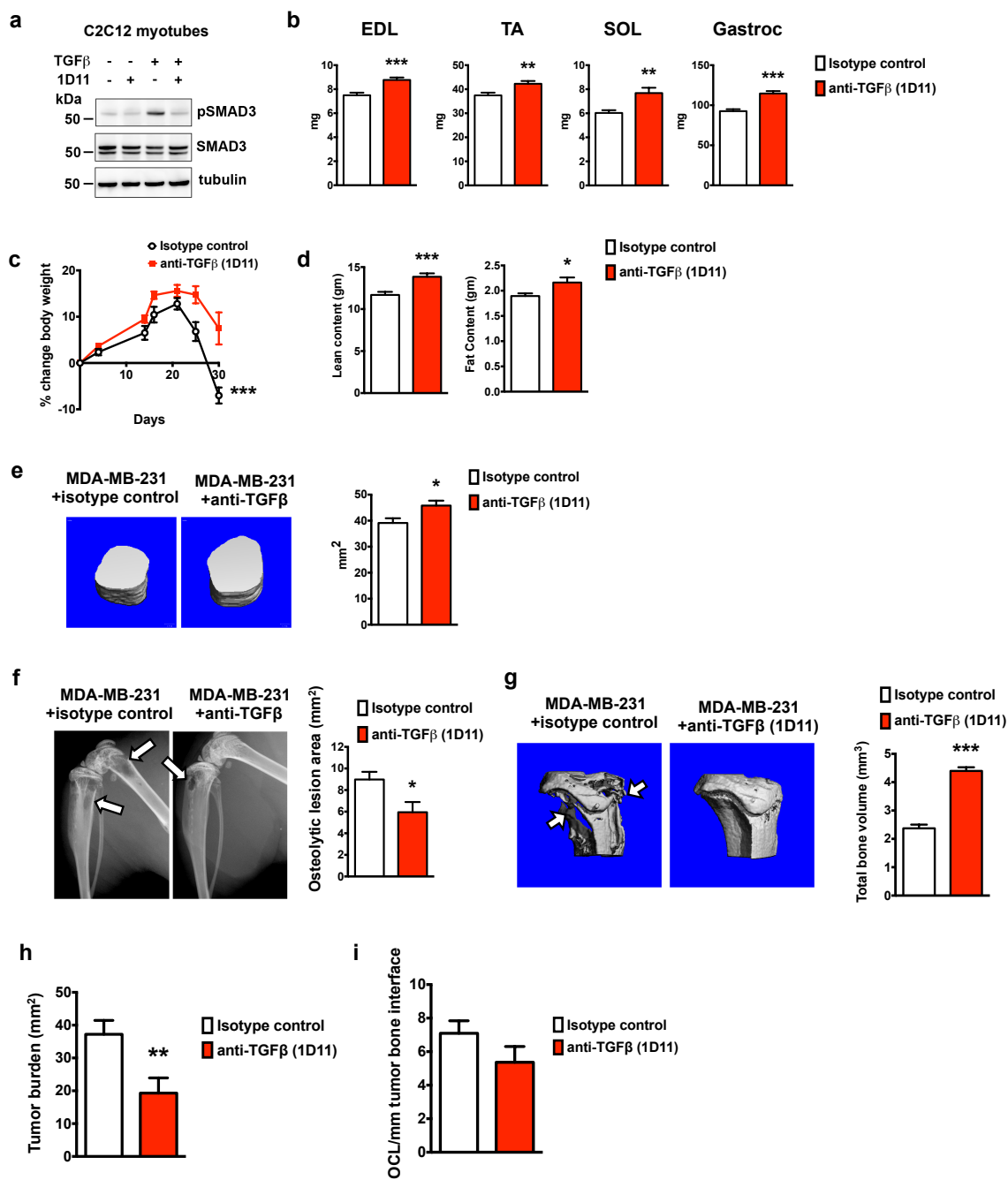
(f) Increased lean and fat content in mice ( $n=13$ ) treated with SD-208, ZA and SD-208+ZA compared to vehicle treated mice.

(g) Increased mid-calf cross-sectional area in mice ( $n=5$ ) treated with SD-208, ZA and SD-208+ZA compared to vehicle treated mice.

(h) Tumor burden ( $\text{mm}^2$ ) was lower in mice treated with SD-208, ZA or SD-208+ZA compared to vehicle treated mice ( $n=10$ ).

(i) Number of osteoclasts per mm of tumor bone interface was lower in mice treated with ZA or SD-208+ZA compared to vehicle treated mice ( $n=3$ ).

Data are mean  $\pm$  s.e.m., (a) t-test; (b,d,f,g,h,i) One-way ANOVA with multiple comparisons; (e) Two-way ANOVA. \* $P<0.05$ , \*\* $P<0.01$ , \*\*\* $P<0.001$ , \*\*\*\* $P<0.0001$ .



## Supplementary Figure 6

Blocking TGF $\beta$  activity with anti-TGF $\beta$  neutralizing antibody (1D11), prevented weight loss, lowered tumor burden and lowered SMAD3 phosphorylation in muscle from mice with bone metastases.

(a) SMAD3 phosphorylation relative to total SMAD3 expression is higher in C2C12 cells treated with TGF $\beta$  and blocked by anti-TGF $\beta$  antibody, 1D11 compared to control cells ( $n=3$ ).

(b) Weight of individual muscles dissected from the lower hindlimb of mice with MDA-MB-231 bone metastases is higher in mice treated with 1D11 compared to isotype control treated mice ( $n=15$ ).

(c) 1D11 reduced loss of body weight over baseline compared to isotype control treated mice in mice ( $n=15$ ) with bone metastases.

(d) 1D11 increased lean and fat content compared to isotype control treated mice in mice ( $n=15$ ) with bone metastases.

(e) Mid-calf cross-sectional area was higher ( $n=5$ ) was increased in mice with MDA-MB-231 bone metastases treated with 1D11 compared to isotype control treated mice .

(f) Osteolytic lesion area was lower ( $n=15$ ) in mice with MDA-MB-231 bone metastases treated with 1D11 compared to isotype control treated mice .

(g) Average tibia total bone volume ( $n=3$ ) was higher in mice with MDA-MB-231 bone metastases treated with 1D11 compared to isotype control treated mice .

(h) Tumor burden ( $\text{mm}^2$ ) was lower in mice treated with 1D11 compared to isotype control treated mice ( $n=13$ ).

(i) The number of osteoclasts per mm of tumor bone interface was not changed in mice treated with 1D11 compared to isotype control treated mice ( $n=11$ ).

Data are mean  $\pm$  s.e.m., (b,d-i) t-test; (c) Two-way ANOVA. \* $P<0.05$ , \*\* $P<0.01$ , \*\*\* $P<0.001$ .



## Supplementary Figure 7

NADPH oxidase expression is associated with RyR1 and inhibiting Nox4 does not prevent tumor growth in bone.

**(a)** left: Relative *Nox1* mRNA expression in TA muscle from non-tumor mice and mice with MDA-MB-231 bone metastases compared to non-tumor control mice ( $n=3$ ). right: Relative *Nox2* mRNA expression ( $n=4$ ) in TA muscle from non-tumor mice and mice with MDA-MB-231 bone metastases compared to non-tumor control mice ( $n=3$ ).

**(b)** top row: Nox4-RyR1 co-IP was higher ( $p=0.0791$ ) in mice with MCF-7 mixed osteolytic/osteoblastic breast cancer bone metastases compared to non-tumor control mice ( $n=4$ ). Higher Nox4-RyR1 co-immunoprecipitation (co-IP) in muscle from mice with A549 osteolytic lung cancer bone metastases compared to non-tumor control mice ( $n=4$ ). Higher Nox4-RyR1 co-immunoprecipitation (co-IP) in muscle from mice with RWGT2 mixed osteolytic/osteoblastic lung cancer bone metastases compared to non-tumor control mice ( $n=4$  each). middle row: Nox4-RyR1 co-IP was higher in mice with PC-3 osteolytic prostate cancer bone metastases compared to non-tumor control mice, and JJN-3 osteolytic multiple myeloma compared to non-tumor control mice ( $n=4$  each). bottom row: In contrast, Nox4-RyR1 co-IP is not altered in mice with primary MDA-MB-231 tumors (without bone metastases) compared to non-tumor control mice or mice with ZR75-1 bone metastases compared to non-tumor control mice ( $n=4$  each).

**(c)** Nox4 inhibitor (GKT137831) did not affect the osteolytic lesion size in mice with MDA-MB-231 bone metastases ( $n=9$ ).

**(d)** GKT137831 did not affect lower hindlimb muscle mass in mice with MDA-MB-231 bone metastases compared to non-tumor control mice ( $n=9$ ).

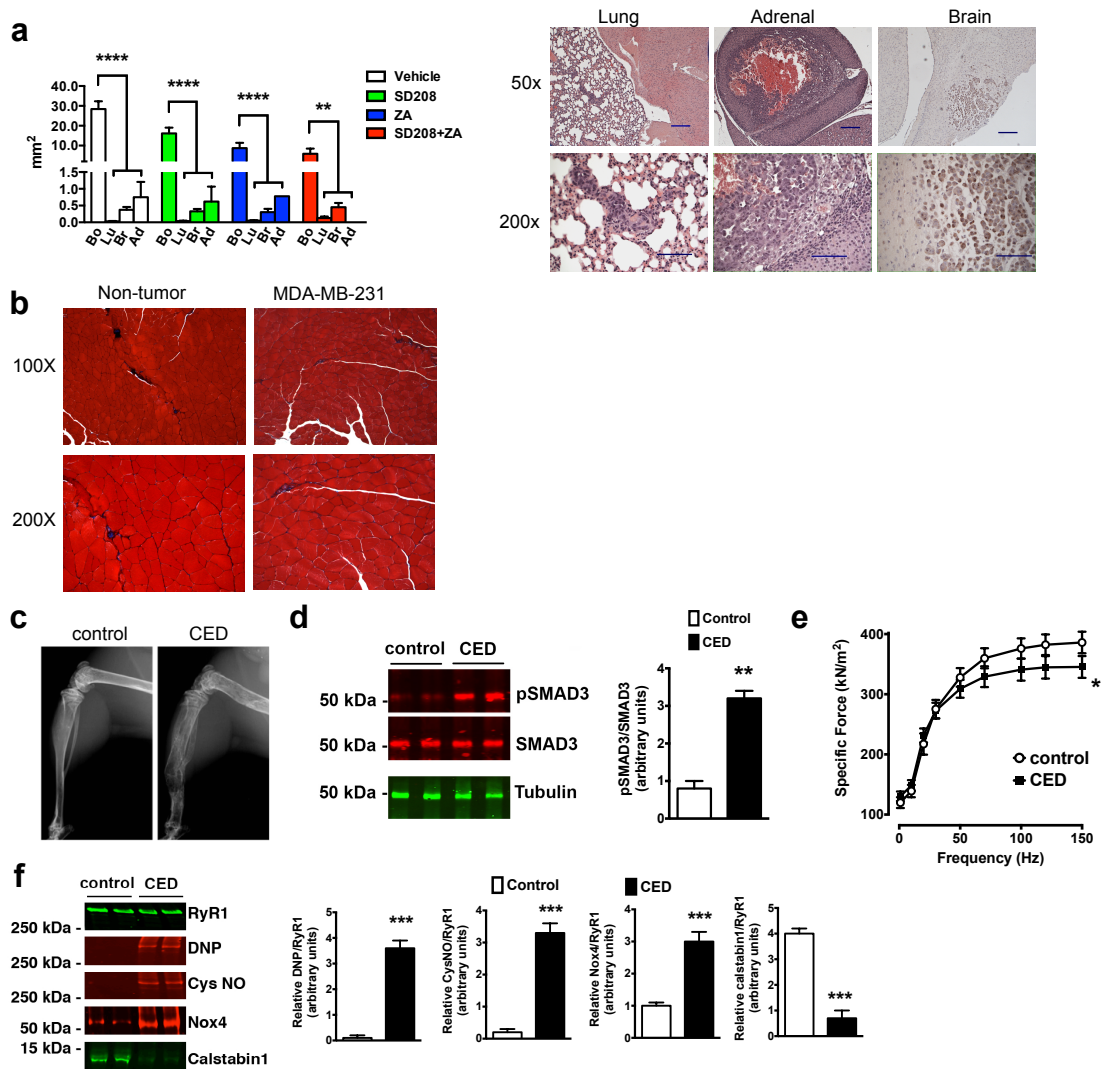
**(e)** GKT137831 did not affect body weight in mice with MDA-MB-231 bone metastases compared to non-tumor control mice ( $n=9$ ).

**(f)** GKT137831 did not affect lean and fat content in mice with MDA-MB-231 bone metastases compared to non-tumor control mice ( $n=9$ ).

**(g)** GKT137831 did not affect mid-calf cross-sectional area in mice with MDA-MB-231 bone metastases compared to non-tumor control mice ( $n=5$ ).

**(h)** GKT137831 did not affect grip strength in mice with MDA-MB-231 bone metastases compared to non-tumor control mice ( $n=9$ ).

Data are mean  $\pm$  s.e.m., **(a,b,c,g)** t-test; **(d,f)** One-way ANOVA; t-test; **(e,h)** Two-way ANOVA. \* $P<0.05$ , \*\* $P<0.01$ , \*\*\* $P<0.001$ , \*\*\*\* $P<0.0001$ .



## Supplementary Figure 8

Tumor burden in lung, brain and adrenal glands is small compared to tumor burden in bone and muscle weakness is not due to fibrotic tissue in muscle. A non-malignant bone metabolic disorder (Camurati-Engelmann [CED]) leads to muscle weakness.

**(a)** Tumor volume in mice with MDA-MB-231 bone metastases measured in bone (Bo), lung (Lu), and adrenal glands (Ad) by H&E staining and in brain (Br) by Ki-67 immunohistochemical staining. Tumor volume in bone is higher than in any other tissue. All values are in mm<sup>2</sup>. Scale bars at 50x are 100µm and at 200x are 50µm.

**(b)** Histology of muscle following staining with Mallory-Heidenhain Azan stain showed no fibrosis in muscle from mice with MDA-MB-231 breast cancer bone metastases compared to non-tumor control mice.

**(c)** CED mice show diaphyseal dysplasia and osteolysis by x-ray.

**(d)** SMAD3 phosphorylation is increased in skeletal muscle from CED mice but not in littermate controls ( $n=4$ ).

**(e)** *Ex vivo* muscle contractility of the extensor digitorum longus (EDL) muscle was lower in CED mice compared to littermate controls ( $n=10$ ).

**(f)** RyR1 was oxidized and nitrosylated and calstabin1 binding was lower in mice with CED ( $n=4$ ). RyR1-Nox4 binding was increased in CED mice compared to littermate controls.

Data are mean  $\pm$  s.e.m., **(a)** Tumor area of grouped soft tissue metastases versus bone metastases. Data analyzed in each group as well as vehicle by t-test. **(d,f)** t-test; **(e)** Two-way ANOVA. \* $P<0.05$ , \*\* $P<0.01$ , \*\*\* $P<0.001$ , \*\*\*\* $P<0.0001$ .

**Supplementary Table 1. Nitrosylated skeletal muscle proteins from mice with MDA-MB-231 bone metastases.**

<b>Gene Name</b>	<b>Protein Name</b>
Myh7b	Myosin-7B
Ttn	Titin
Hspg2	Basement membrane-specific heparan sulfate proteoglycan core protein
Zc3h3	Zinc finger CCCH domain-containing protein 3
Gys1	Glycogen [starch] synthase, muscle
Pikfyve	1-phosphatidylinositol-3-phosphate 5-kinase, Isoform 2
Tpm3	Tropomyosin 3, gamma
<b>Ryr1</b>	<b>Ryanodine receptor</b>
Tbck	TBC domain-containing protein kinase-like protein
Gm7251	Glyceraldehyde-3-phosphate dehydrogenase
Ankrd50	Ankyrin repeat domain 50
Lamc1	Laminin subunit gamma-1
Pcf11	Cleavage and polyadenylation factor subunit homolog
Plin4	Perilipin-4, Isoform 2
Actn3	Alpha-actinin-3
Myl1	Myosin light chain 1/3, skeletal muscle isoform
Surf2	Surfeit locus protein 2
Tpm3	Tropomyosin alpha-3 chain
Ckb	Creatine kinase B-type
Vdac1	Voltage-dependent anion-selective channel protein 1
Tpm4	Tropomyosin alpha-4 chain
Zfyve1	Zinc finger FYVE domain-containing protein 1
Actbl2	Beta-actin-like protein 2
Phlpp2	PH domain leucine-rich repeat-containing protein phosphatase 2
Pappa	Pappalysin-1
Cul7	Cullin-7, Isoform 2
Snrnp200	Activating signal cointegrator 1 complex subunit 3-like 1
Casp8ap2	CASP8-associated protein 2

Total skeletal muscle proteins from MDA-MD-23 mice with bone metastases were analyzed by mass spectroscopy in order to identify nitrosylated proteins.

**Supplementary Table 2. Oxidized skeletal muscle proteins from mice with MDA-MB-231 bone metastases.**

Gene Name	Protein Name
Obscn	Obscurin
Plekhn2	Isoform 3 of Pleckstrin homology domain-containing family M member 2
Fhl1	Four and a half LIM domains protein 1
Tpm2	Tropomyosin beta chain
Atp5c1	ATP synthase subunit gamma, mitochondrial
Capzb	Isoform 3 of F-actin-capping protein subunit beta
Ttn	Titin
Wdr76	Isoform 2 of WD repeat-containing protein 76
Aldoat1	Fructose-bisphosphate aldolase
Hbbt1	Beta-globin
Anxa2	Annexin A2
Ndufs5	NADH dehydrogenase [ubiquinone] iron-sulfur protein 5
St3gal3	CMP-N-acetylneuraminate-beta-1,4-galactoside alpha-2,3-sialyltransferase
Itgb6	Integrin beta-6
Ola1	Obg-like ATPase 1
Crebrf	CREB3 regulatory factor
Mybpc1	Protein Mybpc1
Lypla1	Isoform 2 of Acyl-protein thioesterase 1
Tufm	Isoform 2 of Elongation factor Tu, mitochondrial
Finc	Isoform 2 of Filamin-C
Qdpr	Dihydropteridine reductase
Atp1a2	Sodium/potassium-transporting ATPase subunit alpha-2
Acs1	Long-chain-fatty-acid--CoA ligase 1
Prdx6	Peroxiredoxin 6
Ndufv1	NADH dehydrogenase [ubiquinone] flavoprotein 1, mitochondrial
Pygm	Phosphorylase
Ldb3	Isoform 4 of LIM domain-binding protein 3
Nme2	Nucleoside diphosphate kinase B
<b>Ryr1</b>	<b>Ryanodine receptor 1</b>
Tf	Serotransferrin
Neb	Protein Neb
Mta3	Isoform 2 of Metastasis-associated protein MTA3
Fbxw28	Protein Fbxw28
Myh11	Isoform 2 of Myosin-11
Park2	Isoform 3 of E3 ubiquitin-protein ligase parkin
Trf	Serotransferrin (Fragment)
Agl	Protein Agl
Srbd1	S1 RNA-binding domain-containing protein 1
Pias2	Isoform 5 of E3 SUMO-protein ligase PIAS2

Cyp4f17	MCG14247
Myh2	MCG140437, isoform CRA_d
Ikzf1	DNA-binding protein Ikaros
Ldha	L-lactate dehydrogenase A chain
Prdx5	Isoform Cytoplasmic+peroxisomal of Peroxiredoxin-5, mitochondrial
Ulp1	Protein Ulp1
Atp2a2	Isoform SERCA2A of Sarcoplasmic/endoplasmic reticulum calcium ATPase 2
Adssl1	Isoform 2 of Adenylosuccinate synthetase isozyme 1
Tecta	Isoform 2 of Alpha-tectorin
Bin1	Bin1 protein
Dld	Dihydrolipoyl dehydrogenase, mitochondrial
Gbas	Glioblastoma amplified sequence
Pgam2	Phosphoglycerate mutase 2
Actn3	Alpha-actinin-3
Hba	Hemoglobin subunit alpha
Fabp4	Fatty acid-binding protein, adipocyte
Mb	Myoglobin
Got2	Aspartate aminotransferase, mitochondrial
Myl1	Myosin light chain 1/3, skeletal muscle isoform
Ckm	Creatine kinase M-type
Sod1	Superoxide dismutase [Cu-Zn]
Mdh2	Malate dehydrogenase, mitochondrial
Pgk1	Phosphoglycerate kinase 1
Myh8	Myosin-8
Gpd1	Glycerol-3-phosphate dehydrogenase [NAD(+)], cytoplasmic
Mdh1	Malate dehydrogenase, cytoplasmic
Ca3	Carbonic anhydrase 3
Ldhb	L-lactate dehydrogenase B chain
Eno1	Alpha-enolase
Tpi1	Triosephosphate isomerase
Tnnc2	Troponin C, skeletal muscle
Fkbp1a	Peptidyl-prolyl cis-trans isomerase FKBP1A
Xrcc5	X-ray repair cross-complementing protein 5
Adssl1	Adenylosuccinate synthetase isozyme 1
Des	Desmin
Pdha1	Pyruvate dehydrogenase E1 component subunit alpha, somatic form, mitochondrial
Akr1b1	Aldose reductase
Pfkm	6-phosphofructokinase, muscle type
Slc25a4	ADP/ATP translocase 1
Acadvl	Very long-chain specific acyl-CoA dehydrogenase, mitochondrial
Acadl	Long-chain specific acyl-CoA dehydrogenase, mitochondrial
Pkm	Isoform M1 of Pyruvate kinase PKM
Ndufs6	NADH dehydrogenase [ubiquinone] iron-sulfur protein 6, mitochondrial

Idh2	Isocitrate dehydrogenase [NADP], mitochondrial
Cox6b1	Cytochrome c oxidase subunit 6B1
Eef2	Elongation factor 2
Tpm1	Tropomyosin alpha-1 chain
Acta1	Actin, alpha skeletal muscle
Idh3g	Isocitrate dehydrogenase [NAD] subunit gamma 1, mitochondrial
Mylpf	Myosin regulatory light chain 2, skeletal muscle isoform
Uqcrrh	Cytochrome b-c1 complex subunit 6, mitochondrial
Vcp	Transitional endoplasmic reticulum ATPase
Myh6	Myosin-6
Atp5a1	ATP synthase subunit alpha, mitochondrial
Myom2	Myomesin 2
Trim72	Tripartite motif-containing protein 72
Prss38	Serine protease 38
Mfhas1	Malignant fibrous histiocytoma-amplified sequence 1 homolog
Myh4	Myosin-4
Myh1	Myosin-1
Mybpc2	Myosin-binding protein C, fast-type
Ogdh	Isoform 4 of 2-oxoglutarate dehydrogenase, mitochondrial
Vdac1	Isoform Mt-VDAC1 of Voltage-dependent anion-selective channel protein 1
Prdx2	Peroxiredoxin-2
Hadh	Hydroxyacyl-coenzyme A dehydrogenase, mitochondrial
Notch3	Neurogenic locus notch homolog protein 3
Myom1	Myomesin-1
Il17a	Interleukin-17A
Nomo1	Nodal modulator 1
Tpm4	Tropomyosin alpha-4 chain
Ckmt2	Creatine kinase S-type, mitochondrial
Magi1	Isoform 2 of Membrane-associated guanylate kinase, WW and PDZ domain-containing protein 1
Ndufa12	NADH dehydrogenase [ubiquinone] 1 alpha subcomplex subunit 12
Srl	Sarcolumenin
Olfrr553	Olfactory receptor Olfrr553
Echs1	Enoyl-CoA hydratase, mitochondrial
Pdhx	Pyruvate dehydrogenase protein X component, mitochondrial
Hadha	Trifunctional enzyme subunit alpha, mitochondrial
Zfpm2	Isoform 3 of Zinc finger protein ZFPM2
Pdlim5	PDZ and LIM domain protein 5
Sdha	Succinate dehydrogenase [ubiquinone] flavoprotein subunit, mitochondrial
Acat1	Acetyl-CoA acetyltransferase, mitochondrial
Atp2a1	Sarcoplasmic/endoplasmic reticulum calcium ATPase 1
Arrdc4	Arrestin domain containing 4
Ppargc1b	Isoform 2 of Peroxisome proliferator-activated receptor gamma coactivator 1-beta
Lrp4	Isoform 2 of Low-density lipoprotein receptor-related protein 4

Ndufs1	NADH-ubiquinone oxidoreductase 75 kDa subunit, mitochondrial
Klk6	Kallikrein 6, isoform CRA_a
MacroD1	O-acetyl-ADP-ribose deacetylase MACROD1
Aco2	Aconitate hydratase, mitochondrial
Ndufa10	NADH dehydrogenase [ubiquinone] 1 alpha subcomplex subunit 10, mitochondrial
Etfa	Electron transfer flavoprotein subunit alpha, mitochondrial
Park7	Protein DJ-1
Ndufa5	NADH dehydrogenase [ubiquinone] 1 alpha subcomplex subunit 5
Ndufc2	NADH dehydrogenase [ubiquinone] 1 subunit C2
Sdhb	Succinate dehydrogenase [ubiquinone] iron-sulfur subunit, mitochondrial
Uqcrc1	Cytochrome b-c1 complex subunit 1, mitochondrial
Pdhb	Pyruvate dehydrogenase E1 component subunit beta, mitochondrial
Pgm1	Phosphoglucomutase-1
Cyc1	Isoform 2 of Cytochrome c1, heme protein, mitochondrial
Dlst	Dihydrolipoyllysine-residue succinyltransferase 2-oxoglutarate dehydrogenase, mitochondrial
Idh3a	Isocitrate dehydrogenase [NAD] subunit alpha, mitochondrial
Atp5o	ATP synthase subunit O, mitochondrial
Uqcrc2	Cytochrome b-c1 complex subunit 2, mitochondrial
Ndufa8	NADH dehydrogenase [ubiquinone] 1 alpha subcomplex subunit 8
Actn2	Alpha-actinin-2
Myot	Myotilin
NdrG2	Isoform 2 of Protein NDRG2
Rnd2	Rho-related GTP-binding protein RhoN
Ak1	Isoform 2 of Adenylate kinase isoenzyme 1
Pygm	Glycogen phosphorylase, muscle form
Suc1g1	Succinyl-CoA ligase [ADP/GDP-forming] subunit alpha, mitochondrial

Total skeletal muscle proteins from MDA-MD-23 mice with bone metastases were analyzed by mass spectroscopy in order to identify oxidized proteins.

**Supplementary Table 3. Quantification of oxidation of skeletal muscle proteins from tumor bearing mice**

	Carbonyl Concentration (nmol/mg)
Non-tumor	2.0 ± 0.20
MDA-MB-231 (vehicle)	4.8 ± 0.15**
Primary	2.1 ± 0.22
MCF-7	4.4 ± 0.25**
ZR75-1	2.7 ± 0.21
MDA-MB-231 (vehicle)	5.0 ± 0.31
MDA-MB-231 (S107)	3.9 ± 0.28 <sup>###</sup>
MDA-MB-231 (SD-208)	3.3 ± 0.22 <sup>###</sup>
MDA-MB-231 (ZA)	3.2 ± 0.26 <sup>###</sup>
MDA-MB-231 (SD-208/ZA)	3.1 ± 0.17 <sup>###</sup>
MDA-MB-231 (Isotype control)	5.1 ± 0.27
MDA-MB-231 (Anti-TGFβ)	3.2 ± 0.26 <sup>###</sup>
GKT137831	3.1 ± 0.22 <sup>###</sup>
Non-tumor	2.1 ± 0.23
A549	4.4 ± 0.18 **
RGWT2	4.6 ± 0.31 **
Non-tumor	1.8 ± 0.15
PC3	4.5 ± 0.25 **
JJN-3	4.6 ± 0.26 **
Human Control	1.5 ± 0.17
Human BCa bone mets	3.6 ± 0.22 **

\*\*  $P < 0.05$  compared to Non-Tumor control

###  $P < 0.05$  compared to Vehicle treated MDA-MB-231 mice

Protein carbonyl concentration was determined as described in the online methods. Samples were analyzed in duplicate ( $n=2$  mice from each group).